Electronic structure of the $R_2Ti_2O_7$ (R=Sm–Er, Yb, Lu) oxides

V. V. Nemoshkalenko, S. V. Borisenko, V. N. Uvarov, A. N. Yaresko, A. G. Vakhney, and A. I. Senkevich
Institute of Metal Physics, 36 Vernadskii Street, 252142 Kyiv, Ukraine

T. N. Bondarenko
Institute of Materials Problems, 46 Krzhizhanovsky Street, 252142 Kyiv, Ukraine

V. D. Borisenko
Vinnytsia State Technical University, 95 Khmelnytske Shose, 21021 Vinnytsia, Ukraine
(Received 30 June 2000; published 25 January 2001)

We present the results of the electronic structure investigation for the compounds $R_2Ti_2O_7$ (R=Sm–Er, Yb, Lu) with the pyrochlore-type crystal structure. The methods of x-ray photoelectron and emission spectroscopies, as well as the first-principles band-structure calculations have been employed. A good agreement between theoretical and experimental results was observed. We found considerable influence of the R $5p$ - O $2s$ interaction on the formation of the subvalent bands that has to be taken into account while interpreting experimental data. Estimated values of the optical gaps are closely related to the degree of TiO_6 octahedron distortion.

DOI: 10.1103/PhysRevB.63.075106 PACS number(s): 71.20.−b, 71.28.+d

I. INTRODUCTION

For more than four decades the electronic structure of transition-metal oxides has been attracting great attention arising from their unusual electronic and physical properties. Among this large class of materials, the $A_2B_2O_7$ pyrochlores are of special interest. Many phases where the A and B elements are present in the maximum possible oxidation state demonstrate dielectric, piezo- and ferroelectric behavior.[1–3] Magnetic properties ranging from paramagnetism to ferro- or antiferro-magnetism are encountered in the case when B is a $3d$ transition element and A is a rare-earth metal.[4] Such a variety of properties stimulates wide practical applications of the pyrochlores. Prominent examples are pyrochlore titanates $R_2Ti_2O_7$ (R=Sm–Lu). Demonstrating exceptional insulating and magnetic characteristics, some of these compounds can be used as working substances for a magnetic refrigerator cycling between boiling liquid helium and boiling liquid hydrogen.[5,6] Also, such materials can be treated as model compounds in regard to zirconolite $CaZrTi_2O_7$, which is one of the most effective means of the immobilizing of radioactive nuclear wastes.[7,8] Recently, the pyrochlore rare-earth titanates have been also intensively studied as frustrated antiferromagnets being nearly ideal Ising systems.[9–11]

By investigating the electronic structure of this important class of materials, one can form the basis for understanding the majority of their physical properties. The simultaneous presence of the two types of transition elements and oxygen in the composition makes these objects extremely interesting from the point of view of the fundamental problems of solid state physics. At the same time, simplicity provided by the $3d^0$ electronic configuration of titanium in these substances allows us to apply traditional experimental and computational methods and lets us concentrate our attention on the interplay between structural and electronic structure peculiarities without being involved in the battle with electron-electron correlations.

Nevertheless, the electronic structure of pyrochlore titanates have not been systematically investigated and in order to fill this gap, we initiated the present study. With the help of high-energy spectroscopic methods and computational approaches, we studied the electronic structure of the valence and conduction bands, the origin of the semiconducting gaps, the oxygen-metal chemical bonding, as well as the influence of the crystal structure, and the type of effect the rare-earth element has on the electronic subsystem.

II. CRYSTAL STRUCTURE

Several detailed reviews of the structures and properties of oxide pyrochlores are available.[4,12] Here we mention the general crystallographic characteristics and briefly outline the relevant structure properties in terms of the simple and visual description given in Ref. 13.

Pyrochlores have the chemical composition $R_2Ti_2O_7$ (R=Sm–Lu) and crystallize in the face-centered cubic lattice with the space group $Fd3m$ (O_h^7). The primitive cell comprises two formula units. R and Ti atoms occupy $16d$ ($\frac{1}{2},\frac{1}{2},\frac{1}{2}$) and $16c$ (0,0,0) positions, respectively. A more descriptive formula of the compound is $R_2Ti_2O_6O'$ because six O ($x,\frac{1}{8},\frac{1}{8}$) anions are equivalent, and the seventh O' ($\frac{3}{8},\frac{3}{8},\frac{3}{8}$) anion has a distinct position in the structure. In Table I we summarize the lattice constants and available x parameters that are sufficient to describe the unit cell. Also given in Table I are the nearest R–O and Ti–O distances.

The R^{3+} cations, which are located within oxygen scalenohedra, are eight coordinated (6O+2O'). The Ti^{4+} cations are surrounded by trigonal antiprisms formed by six O atoms. The lanthanide scalenohedron becomes a cube for x =0.375, whereas the Ti trigonal antiprism becomes a perfect octahedron for x=0.3125. Thus, the x parameter can be considered as a measure of the distortion of the oxygen octahedron. In the following, the oxygen atoms forming the dis-

TABLE I. Lattice and available x parameters of $R_2Ti_2O_7$ (R=Sm-Lu).[4] When $x=0.375$, the lanthanide scalenohedra become cubic and when $x=0.3125$, the Ti trigonal antiprisms become perfect octahedra.

Compound	a_0 (Å)	x	$d_{R-O'}$	d_{R-O}	d_{Ti-O}
$Sm_2Ti_2O_7$	10.233	0.327	2.216	2.531	1.973
$Eu_2Ti_2O_7$	10.196	0.327	2.208	2.522	1.966
$Gd_2Ti_2O_7$	10.185	0.322	2.205	2.555	1.944
$Tb_2Ti_2O_7$	10.152				
$Dy_2Ti_2O_7$	10.124	0.323	2.192	2.533	1.936
$Ho_2Ti_2O_7$	10.100				
$Er_2Ti_2O_7$	10.087	0.331	2.184	2.467	1.961
$Yb_2Ti_2O_7$	10.030				
$Lu_2Ti_2O_7$	10.018	0.330	2.169	2.441	1.944

torted TiO_6 octahedra will be referred to as ''titanium oxygens,'' and O' atoms, nearest to the R site, as ''lanthanide oxygens.'' As seen from Table I, a regular TiO_6 octahedron is expected to be a good approximation for most compounds of the series.

The metal sublattice consists of atomic planes that are formed by parallel alternating chains of titanium and rare earth atoms [see Fig. 1(a)]. The chains from neighboring planes are perpendicular. We will consider each type of the oxygen atoms with respect to the nearest metal atom. Since each titanium atom is surrounded by O atoms, the parallel chains of octahedra are generated in accordance with Ti chains [see Fig. 1(b)]. In such a three-dimensional network, the axes of corner shared octahedra make an angle of $\sim 135°$. We see also, that O' atoms accompany R chains giving rise to $R-O'-R$ zig-zags. Located in this way, O' atoms are brought into the centers of the R tetrahedra. Summarizing the description of the structure, we note that although the distortion of TiO_6 octahedra is not vital for understanding the main peculiarities of the crystal structure, it affects substantially the electronic structure. The bigger x parameter, the bigger Ti–O distances and, consequently, the lower R–O distances in a given compound. Even if one compares Ti–O distances in $Gd_2Ti_2O_7$ and $Lu_2Ti_2O_7$, they will be nearly equal, despite 1.6% contraction of the lattice, due to the stronger distortion of the TiO_6 octahedra in the case of R=Lu.

III. METHODOLOGY

A. Experiment

Polycrystalline samples of $R_2Ti_2O_7$ (R=Sm–Er, Yb, Lu) obtained by a coprecipitation method were used in the present work.[14] Preliminary x-ray characterization showed that all compounds are well crystallized and virtually free of structural defects. The x-ray photoemission spectroscopy (XPS) experiments were performed as described elsewhere.[13,15] Energy scale calibration was made with respect to the C 1s level. The energy resolution was about 1.2 eV and the accuracy of determination of the binding energies was about 0.1 eV.

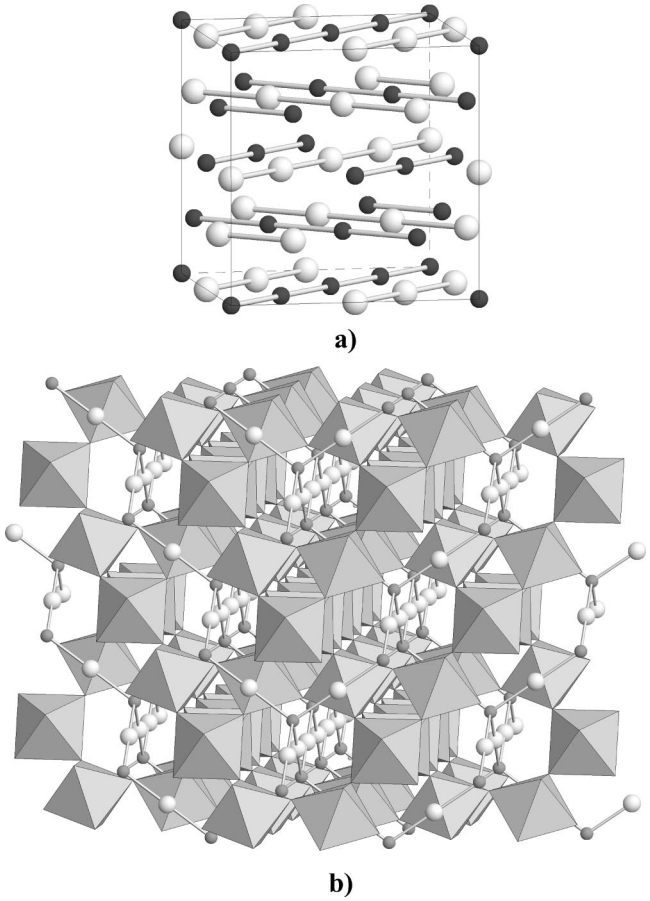

FIG. 1. (a) Metal sublattice in pyrochlores (unit cell). (Only in-plane connection lines are shown.) (b) Crystal structure of $R_2Ti_2O_7$. Light, medium, and dark grey atoms are the lanthanide, oxygen O', and titanium atoms, respectively. Octahedra TiO_6 are distorted as in R=Er compound ($x=0.331$). Octahedra chains and zig-zags can be clearly seen.

Ti $L\alpha$ ($2p\rightarrow 3d4s$ transition) x-ray emission spectra (XES) were measured on the RSM-500 x-ray vacuum spectrometer with a diffraction grating ($N=600$ lines/mm; $R=6$ m) and electron excitation. Ti $K\beta_{2,5}$ ($1s\rightarrow 4p$) emission spectra were obtained using a fluorescent Iohan-type vacuum spectrograph with a quartz single crystal ($10\bar{1}1$ plane) curved to $R=500$ mm as a crystal analyzer. X-ray fluorescence O $K\alpha$ ($1s$-$2p$) spectra were measured on a vacuum spectrometer SARF-1 with the RbAP single crystal ($2d=26.136$ Å, $R=500$ mm). The energy resolution for Ti $L\alpha$, Ti $K\beta_{2,5}$, and O $K\alpha$ spectra was about 1.5 eV, 1.0 eV, and 0.5 eV, respectively. The x-ray emission spectra were brought to the binding energy scale with respect to the Fermi level of the XPS spectrometer analyzer using the measured binding energies of corresponded core levels and Ti$K\alpha_1$ peak position.

B. Computational details

The electronic structure of $R_2Ti_2O_7$ was calculated self-consistently within the framework of the local-density approximation (LDA) to the density-functional theory.[16,17] For

the exchange-correlation potential, the von Barth-Hedin parametrization[18] has been employed.

The band-structure calculations were performed by fully relativistic linear muffin-tin orbital (LMTO) method[19–21] in the atomic-sphere approximation (ASA) with the combined correction term[22] taken into account. Since the crystal structure of $R_2Ti_2O_7$ is not closely packed, which results in a large overlap of the atomic spheres, additional empty spheres were inserted into the corresponding unit cells. The angular momentum decomposition of the basis functions included $l=2$ for lanthanide and titanium and $l=1$ for oxygen and the empty spheres, whereas localized lanthanide $4f$ electrons were treated as corelike states. The calculations were performed using two separate energy panels. The basis set for the upper panel contains R $6p$ states. However, to describe properly the effect of R $5p$–O $2s$ hybridization on the XES spectra, R $5p$ states were included into the basis for the lower panel that spans the energy range of R $5p$ and oxygen $2s$ states. The Brillouin zone integrations in the self-consistency loop were performed using the improved tetrahedron method[23] on a grid of 864 **k** points.

Finally, the exchange splitting of R $4f$ electrons in $R_2Ti_2O_7$ was estimated from scalar relativistic spin polarized LMTO calculations.

IV. RESULTS AND DISCUSSION

We show the valence-band (VB) x-ray photoemission spectra for all compounds of the series in Fig. 2. There are two clearly observed groups of features located in 35–15 eV and 15–0 eV binding-energy regions. Both groups are sensitive to the type of the lanthanide atom and we will discuss corresponding energy intervals separately.

A. Electronic states within 35–15 eV binding-energy region

One can see that below 15 eV, the spectra of the VB of most compounds are composed of three main peaks (marked *A*, *B*, and *C*) which are due to the contributions from R $5p$ and O $2s$ electrons. The structure of the spectra in the given energy interval is complex enough, especially for the beginning of the series. The energy position of the peak *C*, which becomes visible when R=Tb, is only slightly affected by the increase of *R* atomic number, whereas the features *A* and *B* move towards bigger binding energies. Moreover, the intensities and widths of peaks *A*, *B*, and *C* also depend on composition. Precise analysis of their relative intensities is difficult because of the different backgrounds stemming from the superposition of core Ti $3p$ and R $5s$ states. Nevertheless, the energy location of these features proved to be weakly dependent on different background subtractions (± 0.1 eV). Thus, the analysis of the XPS valence-band spectra shows that observed structure cannot be ascribed to the simple superposition of atomiclike O $2s$ and R $5p$ contributions, suggesting the possibility of formation of a chemical bond between R $5p$ and O $2s$ electrons.

In Fig. 3 we compare the energy position of the experimental features *A*, *B*, and *C* with the corresponding peaks A', B', and C' in the total densities of states (DOS) (not shown). The best agreement between the experiment and calculation was achieved by employing fully relativistic version of LMTO-ASA with $5p$ electrons of rare earth being treated as valence electrons. Since such an approach correctly predicts a three-peak structure in this energy range, experimental peak *C* can be ascribed to the oxygen $2s$-derived states, whereas *A* and *B* are due to the R $5p_{1/2}$- and R $5p_{3/2}$-derived spin-doublet components, respectively. Calculations give not only the right value of the spin-doublet splitting for each compound, but also its variation across the series. We note also, that since the energy separation between B' and C' is larger than in the experiment, one should expect an even higher degree of R $5p$ - O'(O) $2s$ interaction than the one predicted by the band-structure calculations.

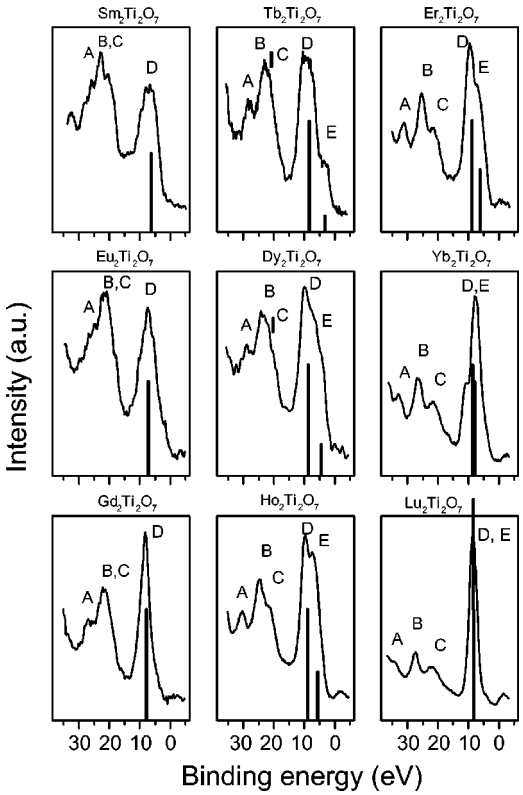

FIG. 2. Experimental valence-band x-ray photoemission spectra of $R_2Ti_2O_7$ (R=Sm–Er, Yb, Lu). If peaks are not clearly resolved or defined, the label contains a comma. Also shown as vertical lines proportional to the occupation numbers are the binding energies of quasicore $4f$ electrons (LMTO-ASA).

To understand in more detail the subvalence band structure, we show in Fig. 4 the evolution of the partial DOS in the given energy interval for the three compounds of the series: the first ($Sm_2Ti_2O_7$), the middle ($Dy_2Ti_2O_7$), and the last ($Lu_2Ti_2O_7$). The partial DOS are grouped in Fig. 4 in accordance with crystal structure fragments. The left column corresponds to the atoms from R–O′–R zig-zags, while the right one represents partial DOS of the TiO_6 octahedra atoms. These latter DOS turn out to be weakly sensitive to the type of lanthanide. Only in the case of R=Sm are detectable features at energies of Sm $5p$ components present. This observation explains the relatively stable binding energy of the experimental peak *C*, which is caused by the titanium oxy-

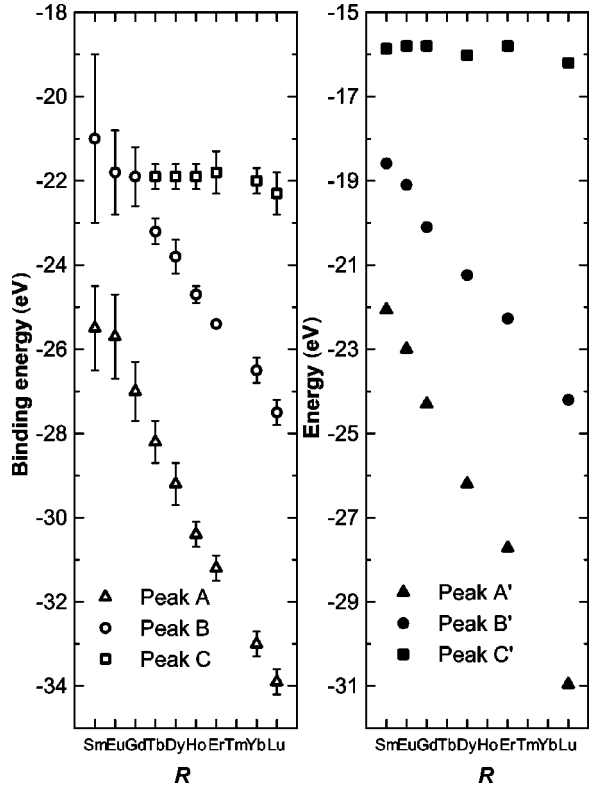

FIG. 3. The energy positions of the peaks corresponding to subvalent states. Left panel: experimental peaks' positions in XPS spectra (Fig. 2). Right panel: the main maxima positions in total DOS.

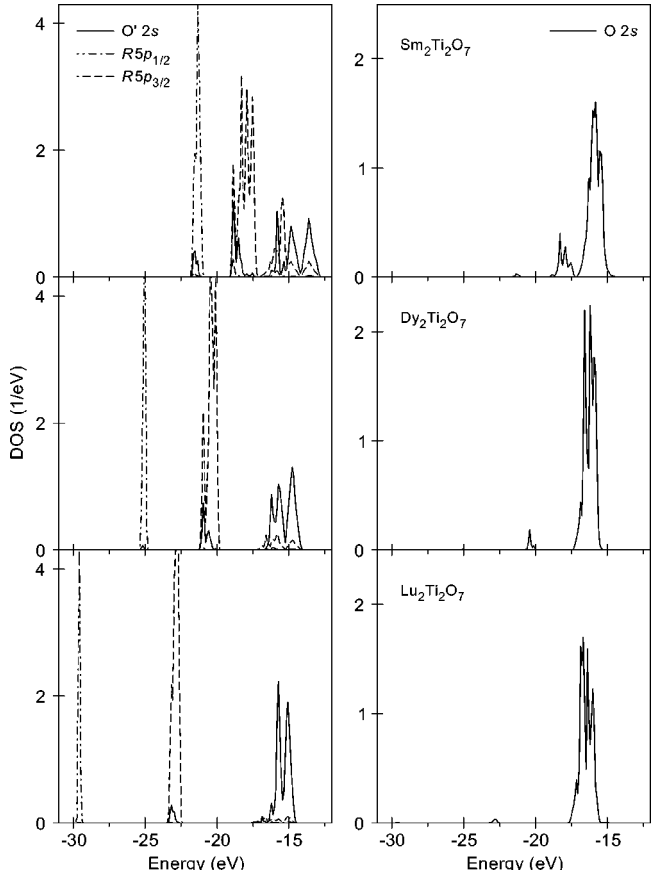

FIG. 4. Dominant partial DOS for $Sm_2Ti_2O_7$, $Dy_2Ti_2O_7$, and $Lu_2Ti_2O_7$ compounds in subvalent energy region (for details, see text).

gen $2s$ electrons rather than O' $2s$ electrons. In contrast, the shape and energy localization of O' $2s$ distribution depend much stronger on the type of rare-earth element. It makes itself evident in the splitting of O' $2s$ states on several components, which is particularly striking for the beginning of the series. Thus, the foregoing suggests that the hybridization of R $5p$ with O' $2s$ is much stronger than R $5p$–O $2s$ hybridization, which can be explained by the fact that the R–O distances are longer than R–O′ ones for all the compounds. The hybridization degree for $5p_{3/2}$-derived states is found to be stronger than for $5p_{1/2}$, which is not unexpected since the energy position of the former is closer to that of oxygen $2s$ states. The interaction in question becomes weaker as the lanthanide atomic number increases. Clearly resolved two components structure remains peculiar to O' $2s$ DOS, thus indicating that it is no longer influenced by the interaction with $5p$ electrons and that it is primarily due to the interaction with R $5d$ and $6s$ electrons. All of the preceding is intended to illustrate that rare-earth $5p$-oxygen $2s$ interaction exists and that it strongly depends on spatial proximity between these atoms, as well as on the type of lanthanide.

It should be pointed out that the inclusion of R $5p$ states into the basis is also crucial for total-energy calculations. It has been found that the calculated equilibrium lattice constants of $R_2Ti_2O_7$ are much closer to the experimental ones if R $5p$ electrons are treated as valence and not as core states.

B. Electronic states within 15–0 eV binding-energy region

Turning back to Fig. 2, one can see that the shape, energy positions, and intensities of the individual spectral features marked D and E undergo noticeable changes upon the change of the R atom. Considering the relative intensities of D and E peaks compared to the higher binding energy spectral weight, one can note that the increase of the lanthanide atomic number (Z_R) results in growth of D from $R=$Sm to $R=$Gd. Feature E appears in the $Tb_2Ti_2O_7$ spectrum and becomes more intense upon further increase of Z_R. This observation suggests that the increasing number of R $4f$ electrons is responsible for such a gain in intensity and shows on the determinative influence of rare-earth $4f$ electrons on the photoemission near the top of the valence band. Comparison of the atomic photoionization cross sections provides support for the previous statement. The ratios $\sigma_{(\mathrm{Sm}\,4f)}/\sigma_{(\mathrm{O}\,2p)}\approx 44$ and $\sigma_{(\mathrm{Sm}\,4f)}/\sigma_{(\mathrm{Ti}\,3d)}\approx 60$ rise through the series and run up to ≈ 340 and ≈ 480, respectively, in the case of $R=$Lu.[24] At the same time, valence-band XPS spectra of the LnF_3 and R_2O_3 (R=La–Lu) compounds obtained in Refs. 25 and 26 demonstrate the similar behavior in 0–15 eV energy range. In other words, R $4f$-derived part of the spectra for the various rare earth compounds with the same ionicity turns out to be weakly sensitive to both lanthanide coordination and crystal structure, suggesting that R $4f$ electrons do not take part

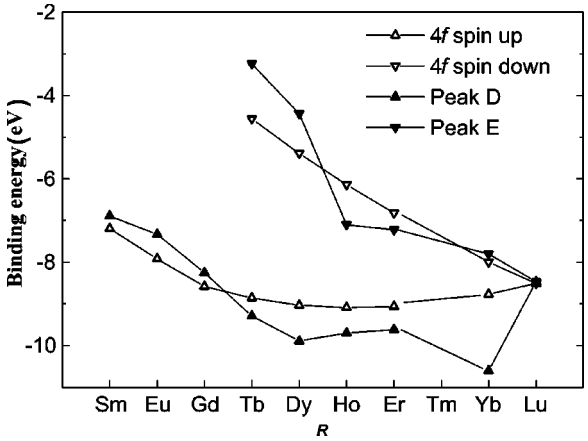

FIG. 5. Experimental peaks' positions in XPS spectra corresponding to $4f$ electrons compared with the computational data.

in the chemical bonding. It is in this assumption the band-structure calculations were performed. Corresponding results are shown in Fig. 2 as vertical lines with their heights being proportional to the occupation numbers of up- and down-spin $4f$ levels. The calculated energies of $4f$ electrons, as well as the energies of peaks *D* and *E*, are presented in Fig. 5. The same shift of 2.4 eV has been applied to all the calculated energies in order to achieve the best agreement between experimental and calculated energy positions. Multiplet splitting determined by the final state after $4f$-electron photoemission has not been taken into account. Nevertheless, as can be seen in Figs. 2 and 5, there is a reasonable correspondence of the calculated energies of $4f\uparrow$ and $4f\downarrow$ levels and the experimental peak positions. Since in the present work we do not address the detailed investigation of R $4f$ electrons, we restrict ourselves to demonstrate that they do not participate in the chemical bonding and that photoemission in the 0–15 eV energy interval is determined by these states.

Since traditional XPS methods do not allow us to investigate the contributions of those valence electrons that form chemical bonding in the 0–15 eV region, we further employ XES and computational methods. On very general grounds, one can expect that O $2p$ hybridized with Ti $3d$ and R $5d$ states will dominate in this energy region. Therefore, we have focused our attention on Ti$L\alpha$ and O$K\alpha$ emission spectra. As dipole selection rules apply for XES, and due to the localized character of the initial core states, our studies probe occupied Ti $3d$ and O $2p$ electronic states. In spite of low occupancy of Ti $4p$ orbitals, Ti$K\beta_{2,5}$ spectra provide valuable information about the electronic states of the ligands surrounding the Ti atom. They were recorded in the present work to gain additional information about the energy distribution of O $2s$ and $2p$ states.

In Fig. 6 we compare the experimental spectra for the case R=Dy with corresponding calculated spectra.[27] For the other compounds of the series, these spectra turned out to be quite similar and are not presented here for brevity. As it is seen from Fig. 6, the overall agreement between the experimental spectra and the calculated ones appears to be good. As expected, Ti$K\beta_{2,5}$ spectrum shows typical structure in the

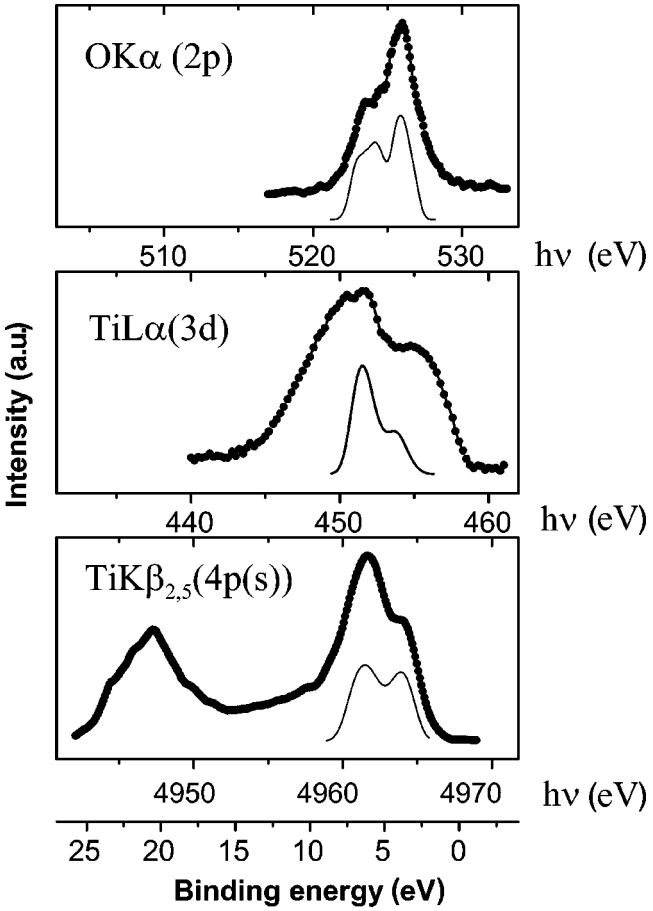

FIG. 6. X-ray emission spectra of $Dy_2Ti_2O_7$ (dots) compared with the calculated spectra (solid lines).

vicinity of 21 eV binding energies that reflects interaction with O$2s$ states. We did not resolve any noticeable differences in this part of the spectrum for different compounds of the series probably not only because of the insufficient energy resolution, but also because ''titanium oxygen'' $2s$ states turned out to be quite inert to the R substitution (see Sec. IVA). The most noticeable differences are the overestimation of the intensity of the lower binding energy feature in Ti$K\beta_{2,5}$ at about 3.8 eV and the width of the Ti$L\alpha$ spectrum. While the former is most likely due to the neglected influence of the energy dependence of the transition matrix elements and a contribution from Ti $4s$ states, the latter is the consequence of the electronic type of excitation used for recording the Ti$L\alpha$ spectrum, which results in the observed widening of the original spectral shape. Nevertheless, presented spectra and the observed correspondence with computational data allow us to extract some information about the structure of the valence band. There are two main features at about 3.8 and 6.4 eV in all the spectra. These features are typical for titanates with perovskitelike lattice,[21] containing TiO_6 octahedra, and indicate the strong hybridization of Ti $3d$ and O $2p$ valence states. It is this interaction that is responsible for the chemical bonding in the distorted titanium-oxygen octahedra in $R_2Ti_2O_7$. The following analysis of the computational results allows us to get additional information regarding the chemical bonding in these compounds.

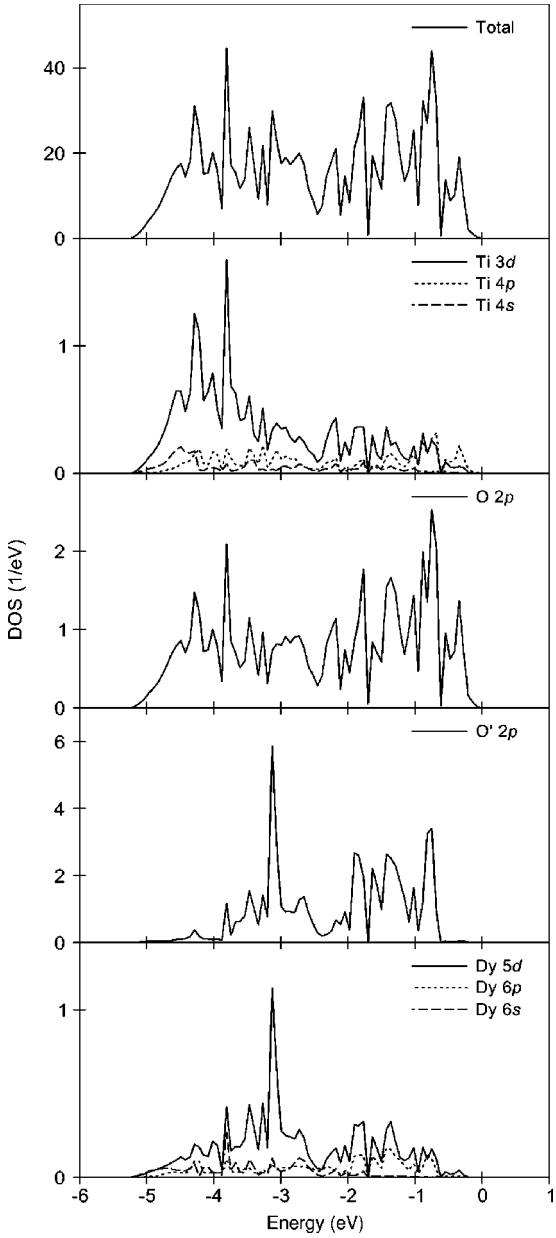

FIG. 7. Total and partial densities of states (DOS) of $Dy_2Ti_2O_7$. Here, and in the following, the total DOS is given per cell, and the partial DOS per atom. Energies are given relative to the valence-band maximum.

As a typical example of the studied pyrochlores, we display in Fig. 7 the calculated total and partial DOS for $Dy_2Ti_2O_7$. There is a broad group of features approximately between -6 and 0 eV. This region is dominantly formed by O $2p$, O' $2p$, Ti $3d$, and Dy $5d$ contributions. The rest of the shown DOS plays only a negligible role in the given energy interval. The states in the energy range from -2.8 to 0 eV are mainly of O $2p$ character with small Ti $3d$ and Dy $5d$ admixture. On the other hand, the d states of both titanium and dysprosium contribute more substantially to the energy range between -5.5 and -2.8 eV. Due to the aforementioned hybridization of Ti d with the O p states, the structure of the Ti d states should follow the density of states of the neighboring oxygen, which is indeed observed in Fig. 7. The same behavior is observed in the case of Dy d and O' p. Their strong resemblance in the given energy range clearly indicates Dy d - O' p hybridization. Partial DOS of the two types of oxygen atoms are different in shape. Moreover, the center of gravity of occupied O' p states lies 0.5 eV deeper than that of O p states. This observation implies that the atomic partial states from the same structural fragment are hybridized between each other more substantially than interfragmentally. It is to be noted that this is valid for all the objects of the series.

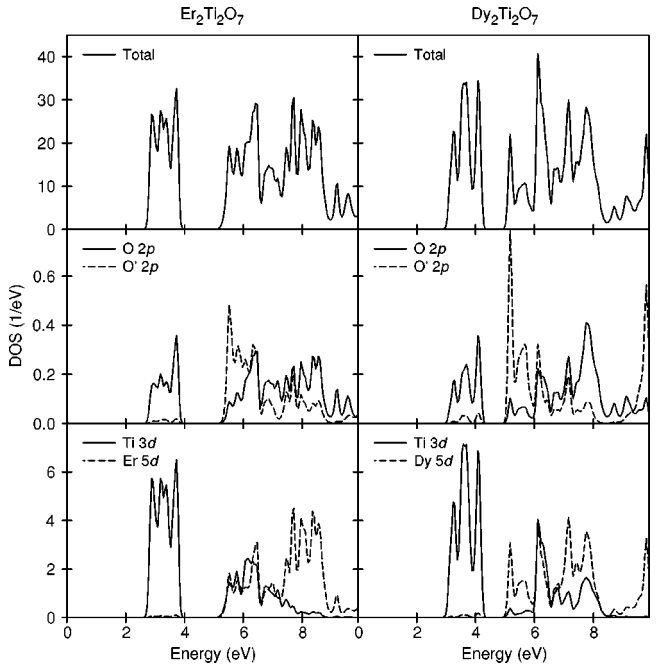

FIG. 8. Total and partial DOS of $Dy_2Ti_2O_7$ and $Er_2Ti_2O_7$. Conduction bands.

C. Electronic states in the conduction band

The valence and conduction band are separated by a direct band gap with the band extrema located in Γ point. In Fig. 8, total and partial DOS are shown for $Er_2Ti_2O_7$ and $Dy_2Ti_2O_7$, which turned out to have minimal 2.63 eV and maximal 2.87 eV values of the gaps, respectively. In contrast to the valence band, the conduction band is more sensitive to the type of lanthanide. The conduction band of all the compounds is split into two sub-bands. The states just above the gap are formed mainly by Ti $3d$ states hybridized with O $2p$ states. These states are separated by a small gap of about 0.8 eV from R $5d$ states that are, in turn, hybridized with $2p$ states of O'. One can note that, as mentioned above, the hybridization within the structural fragments is stronger than interfragmental interaction. However, there is a noticeable Ti $3d$ – R $5d$ hybridization via oxygen $2p$ states. The fact that the energy position of R $5d$ states remains unchanged through the series indicates that the excessive R nuclear charge ''seen'' by these electrons is almost perfectly screened by localized R $4f$ electrons.

Again, we observe the hybridization between oxygen (O, O') p and metal (R, Ti) d states with enhanced R $5d$-O $2p$

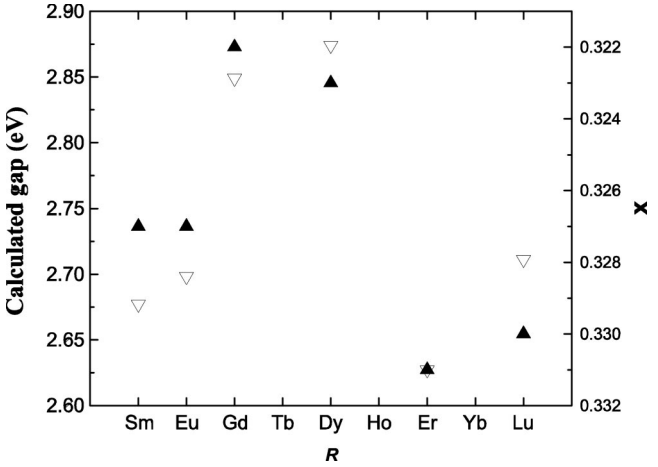

FIG. 9. Calculated optical band gaps (open down triangles) and distortion parameter x (solid up triangles).

interaction in comparison with such interaction of occupied states. However, in contrast to the valence band, the conduction bands are formed primarily by Ti $3d$ and R $5d$ unoccupied states. Presented partial DOS suggest that upper and lower conduction bands are derived from R $5d$ and Ti $3d$ states, respectively. From this observation it is clear that the second gap becomes smaller because of the downshift of R $5d$–O' $2p$–O $2p$ derived states and upshift of Ti $3d$–O $2p$ as one goes from R=Sm, Eu, Er, Lu, to R=Gd, Dy. These shifts can be attributed to the increasing overlap of the Ti $3d$ with the O $2p$ orbitals and simultaneously decreasing R $5d$–O $2p$ overlap. Indeed, the transition from the second group of compounds to the first one is accompanied by the increase of Ti-O distances (and hence, the decrease of R-O distances) due to the stronger distortion of regular TiO_6 octahedra (see Table I).

Therefore, one should naturally expect a very close relation between the calculated gap and the distortion of the TiO_6 octahedra. Data shown in Fig. 9 confirm that the behavior of calculated optical gaps is governed by the value of the distortion parameter x. The stronger the deviation of the TiO_6 antiprism from octahedron, the larger the Ti-O distances and, consequently, the smaller the band gap. The remaining deviation from the inverse proportionality is explained by the change of the lattice constant upon the change of the R atom. The effect of the lattice squeezing due to the substitution of a lanthanide atom by another one with a higher atomic number and a smaller ionic radius can be clearly seen from the comparison of the band gaps of isostructural compounds with R=Sm and R=Eu, which possess the same degree of TiO_6 octahedra distortion. The difference in the gap values is approximately equal to 20 meV.

From the other side, by fixing the atomic number of the lanthanide atom one can investigate the dependence of the gap on the x parameter. Starting from the perfect octahedral coordination of Ti atom (x=0.3125) in hypothetical compound and going to the ideal cubic coordination of the R atom (x=0.375) one can easily predict a reduction of the gap value. Indeed, model calculations for $Gd_2Ti_2O_7$ not only confirm this behavior but also indicate the presence of the insulator-metal transition that occurs at $x \approx 0.37$, which is very close to the perfect LnO_8 cubes.

V. CONCLUSION

In summary, we have investigated electronic structure of ternary oxides $R_2Ti_2O_7$ (R=Sm–Er, Yb, Lu) with the help of experimental XPS and XES measurements and *ab initio* calculations. The calculated spectral features agree well with the experimental ones for all compounds of the series. XPS spectra near the top of the valence band are strongly influenced by Ln$4f$ contributions and do not allow us to determine the role of other electrons in the formation of this energy region. Lanthanide $4f$ states are assumed to be not hybridized with the other states and could be well described as spin-polarized quasicore states. XES and computational results show that the 0–15 eV region of the valence band is formed primarily by oxygen $2p$, titanium $3d$, and lanthanide $5d$ electrons. Considering the crystal structure of pyrochlores as a superposition of TiO_6 octahedra chains and R–O′–R zig-zags, we found out that the atomic partial states from the same structural fragment are hybridized between each other more substantially than interfragmentally. On the basis of XPS data and fully relativistic LDA calculations, it was shown that there is a hybridization between subvalent R $5p$ and O $2s$ states. The degree of this interaction depends on the sort of lanthanide as well as the R–O distance and symmetry of an R nearest neighborhood. The values of the optical band gaps have been estimated from spin restricted fully relativistic LMTO-ASA calculations using experimental crystal structure information. Ranging from 2.63 eV ($Er_2Ti_2O_7$) to 2.87 eV ($Dy_2Ti_2O_7$) the gap values turned out to be closely related to the degree of TiO_6 octahedron distortion. In all investigated compounds, the decrease of the Ti $3d$–O $2p$ bonding-antibonding splitting not only reduces the gap value but also results in the appearance of a split-off conduction band right above the optical band gap.

[1] J. E. Greedan, J. N. Reimers, C. V. Stager, and S. L. Penny, Phys. Rev. B **43**, 5682 (1991).
[2] J. E. Greedan and N. P. Raju, Phys. Rev. B **54**, 7189 (1996).
[3] B. D. Gaulin, J. N. Reimers, T. E. Mason, J. E. Greedan, and Z. Tun, Phys. Rev. Lett. **69**, 3244 (1992).
[4] M. A. Subramanian, G. Aravamudan, and G. V. Subba Rao, Prog. Solid State Chem. **15**, 55 (1983).
[5] I. H. Brixner, Inorg. Chem. **3**, 1065 (1964).
[6] D. J. Flood, J. Appl. Phys. **45**, 4041 (1974).
[7] A. E. Ringwood, S. E. Kesson, N. G. Ware, W. Hibberson, and A. Major, Nature (London) **278**, 219 (1979).
[8] H. J. Rossel, Nature (London) **283**, 282 (1980).
[9] M. J. Harris, S. T. Bramwell, D. F. McMorrow, T. Zeiske, and K. W. Godfrey, Phys. Rev. Lett. **79**, 2554 (1997).

[10] J. S. Gardner, S. R. Dunsiger, B. D. Gaulin, M. J. P. Gingras, J. E. Greedan, R. F. Kiefl, M. D. Lumsden, W. A. MacFarlane, N. P. Raju, J. E. Sonier, I. Swainson, and Z. Tun, Phys. Rev. Lett. **82**, 1012 (1999).

[11] R. Siddharthan, B. S. Shastry, A. P. Ramirez, A. Hayashi, R. J. Cava, and S. Rosenkranz, Phys. Rev. Lett. **83**, 1854 (1999).

[12] L. G. Shcherbakova, L. G. Mamsurova, and G. E. Sukhanova, Russ. Chem. Rev. **48**, 423 (1979).

[13] V. V. Nemoshkalenko, V. N. Uvarov, S. V. Borisenko, A. I. Senkevich, and T. N. Bondarenko, J. Electron Spectrosc. Relat. Phenom. **88–91**, 385 (1998).

[14] A. M. Sych and T. V. Novik, Zh. Neorg. Khim. **22**, 68 (1977).

[15] V. V. Nemoshkalenko and A. G. Aleshin, in *Electron Spectroscopy of Crystals* (Plenum, New York, 1979).

[16] P. Hohenberg and W. Kohn, Phys. Rev. **136**, B864 (1964).

[17] W. Kohn and L. J. Sham, Phys. Rev. **140**, A1133 (1965).

[18] U. von Barth and L. A. Hedin, J. Phys. C **5**, 1629 (1972).

[19] O. K. Andersen, Phys. Rev. B **12**, 3060 (1975).

[20] V. V. Nemoshkalenko, A. A. Krasovsky, V. N. Antonov, Vl. N. Antonov, U. Fleck, H. Wonn, and P. Ziesche, Phys. Status Solidi B **120**, 283 (1982).

[21] V. V. Nemoshkalenko and V. N. Antonov, in *Computational Methods in Solid State Physics* (Gordon and Breach, New York, 1998).

[22] O. K. Andersen, O. Jepsen, and D. Glötzel, in *Highlights of Condensed-Matter Theory*, edited by F. Bassani, F. Fumi, and M.P. Tosi (North-Holland, New York, 1985).

[23] P. E. Blöchl, O. Jepsen, and O. K. Andersen, Phys. Rev. B **49**, 16 223 (1994).

[24] J. H. Scofield, J. Electron Spectrosc. Relat. Phenom. **8**, 129 (1976).

[25] Yu. A. Teterin, A. S. Baev, and S. G. Gagarin, Radiokhimiya **28**, 318 (1986).

[26] Yu. A. Teterin, V. M. Kulakov, A. L. Gubskiy, A. P. Kovtun, S. B. Pirkes, G. N. Makushova, and T. A. Krasovskaya, Dokl. Akad. Nauk SSSR **259**, 416 (1981) [Sov. Phys. Dokl. **26**, 1346 (1981)].

[27] Calculated spectra were obtained from the corresponding partial DOS shown in Fig. 7. Oxygen $K\alpha$ spectrum is the weighted (1:6) sum of $O'2p$ and $O2p$ partial DOS. All spectra were broadened to account for the widths of the core levels and shifted by 2.7 eV to achieve the best agreement with the experiment.